M. Nandagopal*, P. Parameswaran, V.D. Vijayanand, S. Panneerselvi,
K. Laha and M.D. Mathew

Recrystalization Behavior of Coldworked 14Cr-15Ni-2Mo Austenitic Stainless Steel Under Tensile Deformation

Abstract: Recrystallization behavior of 20% coldworked alloy D9 (14Cr-15Ni-2Mo austenitic stainless steel) during high temperature tensile deformation has been assessed. The alloy was produced by vacuum induction melting followed either by vacuum arc refining (VAR) or electroslag refining (ESR). Tensile studies were carried out at various temperatures between ambient and 1073 K at an interval of 50 K and at strain rate of 1.2×10^{-3} s^{-1}. The peak in the stress-strain curve was observed for the tensile tests conducted at 973–1073 K. This is attributed to dynamic recrystallization during tensile deformation. The values of the apparent activation energy were estimated as 384 kJ/mol for ESR grade alloy D9 and 372 kJ/mol for VAR grade alloy D9 by hyperbolic-sine Arrhenius equation, which agree well with that required for dynamic recrystallization in stainless steels. TEM studies confirmed extensive recovery and dynamic recrystalization in both the alloys.

Keywords: dynamic recrystallization, activation energy, Zener-Holloman Parameter, VAR and ESR steel

PACS® (2010). 62.20.M-

***Corresponding author: M. Nandagopal:** Mechanical Metallurgy Division, Indira Gandhi Centre for Atomic Research, Kalpakkam 603 102, Tamil Nadu, India. E-mail: nanda@igcar.gov.in
P. Parameswaran, V.D. Vijayanand, S. Panneerselvi, K. Laha, M.D. Mathew: Mechanical Metallurgy Division, Indira Gandhi Centre for Atomic Research, Kalpakkam – 603 102, Tamilnadu, India

1 Introduction

A titanium-modified 14Cr-15Ni-2Mo austenitic stainless steel, known as alloy D9, has been chosen as the material for the fuel cladding and hexagonal wrapper of the Prototype Fast Breeder Reactor [PFBR] presently under construction at Kalpakkam. Core materials in fast breeder reactors are subjected to a high dose of energetic neutrons which lead to profound changes in physical and mechanical properties [1]. One primary form of radiation damage is the displacement damage in which atoms are knocked out from their normal lattice positions producing vacancies and interstitials. The important phenomena arising out of irradiation defects is the change in dimensions generally referred as void swelling, irradiation creep and embrittlement. The mechanical stability of the core components is profoundly affected by this phenomenon. Extensive studies have been carried out [2] to determine the influence of chemical composition and microstructure on the void swelling behaviour of austenitic stainless steels. Compositional adjustment of AISI type 316 stainless steel in terms of decreasing Cr and increasing Ni, led to the development of a 14Cr-15Ni-2Mo steel designated as Alloy D9. Coldwork and grain size refinement were also found to be effective in suppressing swelling [3].

In PFBR, the fuel clad tubes experience temperatures in the range of 673–973 K under steady state operating conditions. Under transient conditions, (due to failure of pumps, rupture of pump to grid plate pipe, uncontrolled withdrawal of control rod etc.), the temperatures can rise upto 1273 K. For target burn-up of 100,000 MWd/t, the maximum neutron dose is 85 dpa (displacements per atom, i.e., the number of times an atom is displaced from its lattice site). Considering the elevated temperature service and influence of irradiation induced stresses, high temperature mechanical properties are essential to be studied. As the alloy constitution profoundly influences tensile behavior, two different methods of refining were chosen and a comparative study is made. Further, microstructural changes during and after high temperature deformation are noteworthy because of their influence on mechanical properties of materials. The processes such as dynamic recovery, dynamic recrystallization and static recrystallization can have a significant effect on the microstructure of the deformed material. The influence of steel melting processes on the mechanical properties of alloy D9 is discussed in our earlier study [4]. Yield strength values of ESR grade material are about 85% of the yield strength values of VAR grade material, the Ultimate Tensile Strength values are about 90% of the Ultimate

Tensile Strength of the VAR grade material. This shows that there is only a little influence in cleanliness, on the strength values of the steel. In the present study the recrystallization behaviour of the steel during tensile deformation and how such behaviour is influenced by melting methods, are studied.

Dynamic recrystallization is the process during which dislocation free grains form, in the materials with low to medium stacking fault energy. More specifically called as discontinuous dynamic recrystallization [5] it occurs after some critical strain ε_c, at high temperature due to straining of metals. The stress-strain response changes from strain hardening to recovery and then to dynamic recrystallization in the case of metals of low stacking fault energy [6]. When critical strain is reached, dynamic recrystallization dominates – while strain hardening and recovery are less effective as principle mechanisms of the stress-strain response. In a stress-strain curve, the onset of dynamic recrystallization can be recognized by a distinct peak in the flow stress, due to the softening effect of recrystallization. The onset of such a deformation mechanism can also be detected from inflection point in plots of the strain hardening rate against stress. It has been shown that this technique can be used to establish the occurrence of the same when this cannot be determined unambiguously from the shape of the flow curve.

2 Experimental

Two heats of alloy D9 were produced by MIDHANI, Hyderabad, India. The alloys were melted by vacuum induction melting followed either by vacuum arc refining or by electroslag refining. Chemical compositions of the alloy D9 are shown in Table 1. Tensile tests were conducted at ambient temperature and in the temperature range 523–1023 K at an interval of 50 K at a strain rate of 1.2×10^{-3} s^{-1}. The test temperature was controlled within ±2 K. Microstructural characterization was carried out by standard metallographic practice using 60% nitric acid solution as etchant. The grain size measured in case of ESR steel is 67 µm and that of VAR steel is 25 µm. Transmission Electron Microscope (TEM) investigations were carried out for evidences of dynamic recrystallization. Electrolytic etching for TEM samples was carried out using dual jet elecropolishing technique. The polishing was carried out at ~20 V in a medium containing one percent perchloric acid and four parts of ethanol. Temperature of the bath was maintained at ~230 K during electropolishing.

Table 1: Chemical composition of ESR and VAR grade alloy D9 SS (in wt%)

Element	ESR grade	VAR Grade
Chromium	13.58	13.88
Nickel	15.12	15.24
Manganese	1.9	2.12
Molybdenum	2.24	2.12
Carbon	0.04	0.045
Titanium	0.23	0.23
Phosphorous	0.005	<0.005
Sulphur	0.003	<0.005
Silicon	0.71	0.64
Cobalt	0.007	0.007
Vanadium	0.02	<0.01
Copper	0.012	0.017
Aluminum	0.018	0.01
Arsenic	<0.0005	0.0019
Niobium	<0.02	<0.005
Tantulum	0.02	<0.01
Boron	<0.001	12 ppm
Nitrogen	0.0077	0.0021
Iron	Balance	Balance

3 Results and discussion

Table 2 shows the dynamic strain ageing (DSA) and Dynamic Recrystallization regions (DRX) for both the steels i.e. the ranges of temperatures in which the steels exhibit dynamic strain ageing and dynamic recrystalli-

Table 2: DSA and DRX regions of ESR and VAR steels

Designation	300–523 K	573–823 K
ESR	No serrations	Type A serrations
	No dynamic recrystallization	
	873–923 K	973–1073 K
	Type A + B serrations	No serrations
	Dynamic recrystallization	
VAR	300–723 K	773–823 K
	No serrations	Type A serrations
	No dynamic recrystallization	
	873 K	923–1073 K
	Type A + B serrations	No serrations
	Dynamic recrystallization	

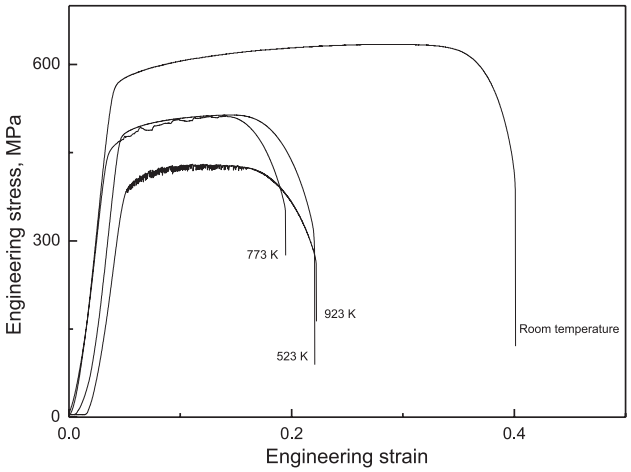

Fig. 1: Engineering stress-strain curves of ESR grade stainless steel.

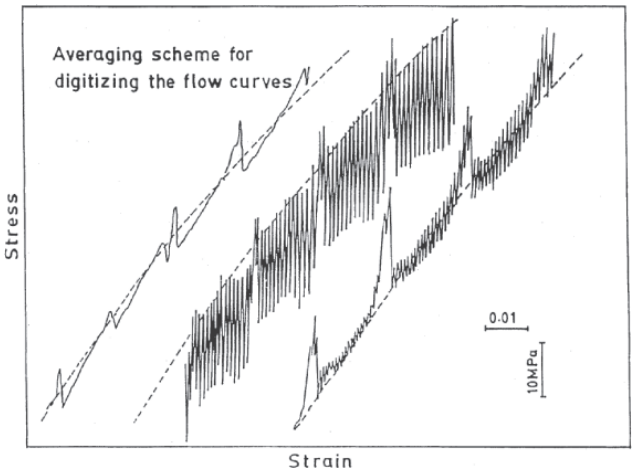

Fig. 3: A schematic showing the smoothening and averaging procedure used for serrated stress strain curves.

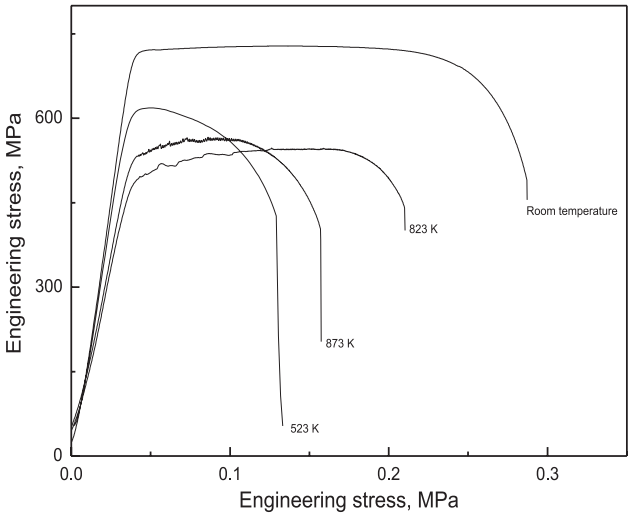

Fig. 2: Engineering stress-strain curves of VAR grade stainless steel.

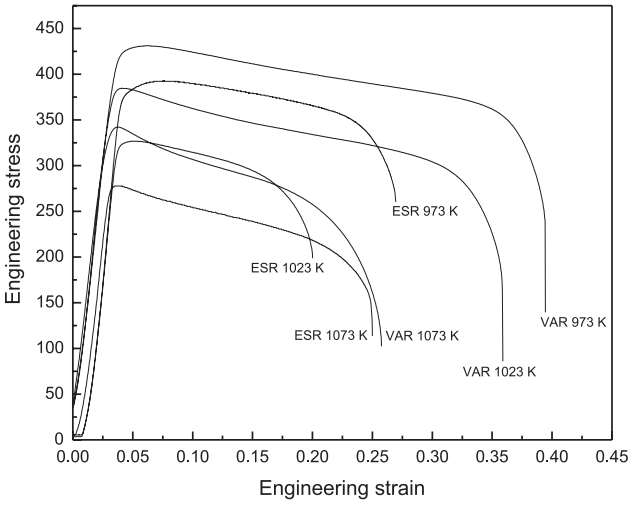

Fig. 4: Typical curves in the DRX regime of ESR and VAR stainless steels.

zation are tabulated. Figs. 1 and 2 show the engineering stress-strain curves of the ESR grade alloy D9 stainless steel and VAR grade alloy D9 stainless steel respectively. Repeated pinning of moving dislocations while arrested at obstacles during plastic straining called as dynamic strain ageing (DSA) is observed in both the steels in the intermediate temperature range [7]. Figure 3 shows the smoothening and averaging procedure used for serrated stress strain curves [8].

Figure 4 shows the stress-strain curves of the ESR and VAR grade stainless steel in the DRX regime. Both the steels show a distinct peak in the stress-strain curve at 973, 1023 and 1073 K. As expected, the strength of the alloy decreased with increase in temperature. The peak observed in the stress-strain curve for the tests conducted at 973–1073 K is often attributed to dynamic recrystallization occurring in this material. The activation energy for dynamic recrystallization was evaluated, using the hyperbolic-sine Arrhenius equation $\dot{\varepsilon} = A[\sinh(\alpha\sigma_p)]^n \exp(\frac{-Q}{RT})$ where $\dot{\varepsilon}$ is the strain rate, A and n are constants, T is the deformation temperature, R the universal gas constant, σ_p is the ultimate tensile stress and Q is the activation energy. From the above equation, we can write $\ln \sinh(\alpha\sigma_p) = -\frac{1}{n} \ln A + \frac{1}{n} \ln \dot{\varepsilon} + \frac{1}{n} \frac{Q}{RT}$ where α is the stress multiplier that provides

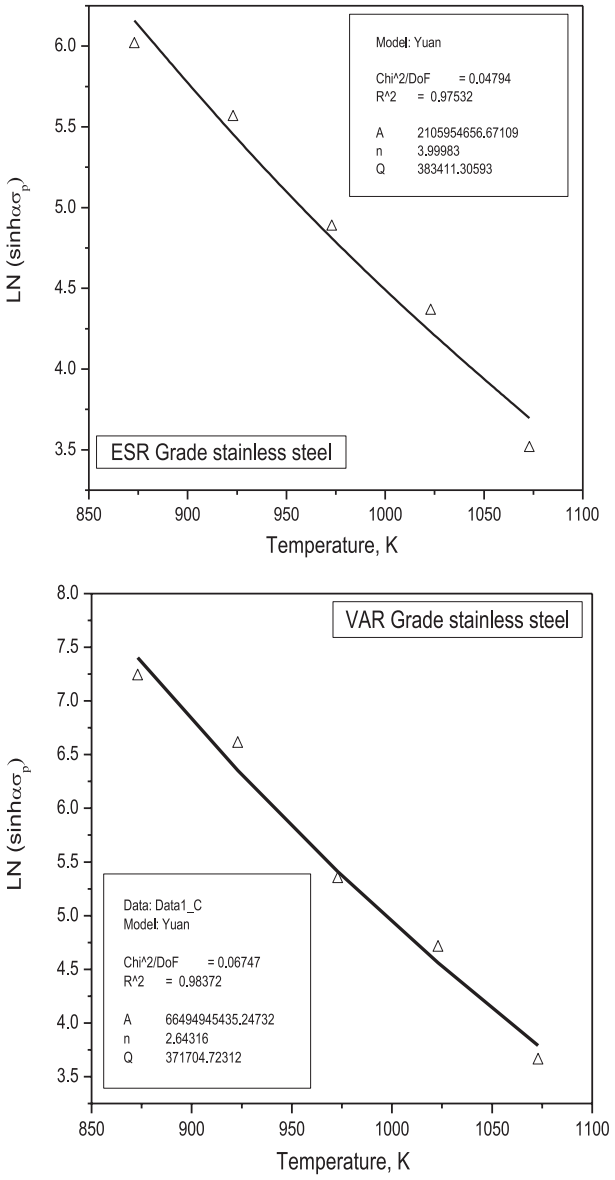

Fig. 5: Plot of ln sinh($\alpha\sigma_p$) vs. temperature.

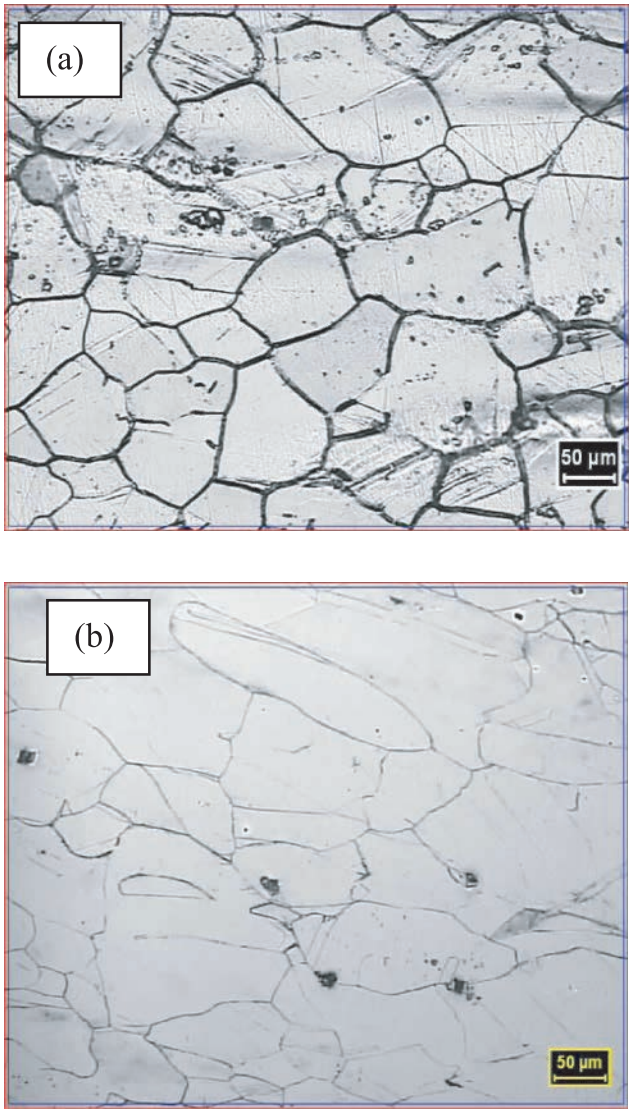

Fig. 6: Optical micrograph of ESR grade SS; (a) 20% coldworked condition and (b) after tensile testing at 1023 K.

an adjustable constant. The value used in our study is 0.014 MPa^{-1}. Figure 5 shows the plots of ln sinh($\alpha\sigma_p$) against temperature for ESR and VAR grade stainless steels respectively. The values of A, n and Q were found to be: $A = 2.1 \times 10^9$ s^{-1}, $n = 4.0$ and $Q = 384$ kJ/mol for ESR grade stainless steel and $A = 6.6 \times 10^9$ s^{-1}, $n = 2.64$ and $Q = 372$ kJ/mol for VAR grade stainless steel. These values agree well with that required for dynamic recrystallization [9] (376–460 kJ/mol). In order to substantiate the occurrence of dynamic recrystallization, microscopy was carried out. The optical micrographs of ESR grade stainless steel and VAR grade stainless steel are shown in Figs. 6 and 7 respectively. Optical micrographs of both the steel show no evidence of recrystallization. Therefore extensive electron microscopy was carried out. Figure 8(a) shows defect dominated elongated cells. During high temperature tensile deformation, the grains resist deformation; the recovery process operates and relieves the stress in the grain resulting in elongated cells. Figure 8(b) shows the wavy nature of grain boundaries, i.e. serrated grain boundaries, which is a signature of dynamic recrystallization [10, 11]. During deformation the grains will be flattened until the boundaries on each side are separated by a small distance. Further the deformation is accompanied by the serration of the grain boundaries where they are in contact with low-angle grain boundaries belonging to sub-grains. Eventually the points of the serrations will come into contact. Figure 8(c) shows the formation of sub

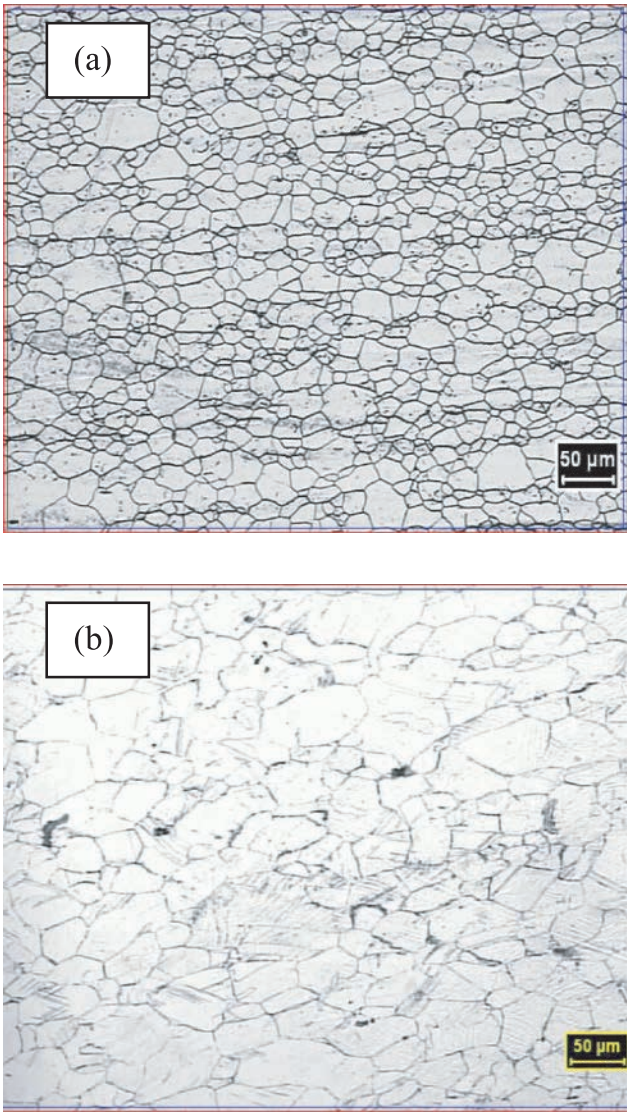

Fig. 7: Optical micrograph of VAR grade SS; (a) 20% coldworked condition and (b) after tensile testing at 1023 K.

grains along the wavy grain boundary. Figure 8(d) shows fine recrystallized grains with moire fringes around its edge.

Inclusions in VAR steel are confined to a very few, well dispersed sulphides, oxides and sometimes silicates. ESR method improves the cleanliness of the steel. But micro inclusions are not removed to the extent in ESR steel as that in VAR steel. These micro inclusions in ESR steel are responsible for recrystallization by pinning low angle and high angle grain boundaries. However ESR method is more effective in decreasing the inclusion content (large particles) in view of the close contact between molten steel droplets and the flux. The deformation fields around these large particles in the case of VAR steel play a major role by acting as ideal sites for the development of recrystallization nuclei. Thus only inclusions viz., micro inclusions or large particles determine the recrystallization behaviour in the case of ESR and VAR steels. Therefore it may be concluded that grain size does not have any dominant role for causing the difference in the recrystallization behaviour. However smaller grain size as in the case of VAR steel increases the critical strain required for DRX, there by delaying the process. Also, the smaller grain size may influence the nucleation behavior and hence delays the onset of dynamic recrystallization, or smaller grain size results in higher work hardening rate and hence delay in the onset of dynamic recrystallization.

Several mechanisms such as dynamic recrystallization (DRX), dynamic strain aging (DSA) and flow localization may cause serrations [12]. DRX considered to be the main mechanism during high temperature deformation, is related to the size of inclusions in the present study. Nevertheless there is no evidence to show that the serrations affect the mechanism of recrystallization and hence the activation energy. However a detailed study is still need to be carried out. But it is evident from the values of activation energy for recrystallization of the both the steels, that DRX occurs in this steel at the temperatures where DSA also occurs.

The flow curves are plotted using θ (work hardening rate) against stress (Figs. 9 and 10) for ESR and VAR in the non-DRX and DRX regimes. In the DRX regime, the curves consist of two stages. While dynamic recovery is the dominant process in the first stage, dynamic recrystallization marked by a change in slope is operative in the second stage. Figures 11 and 12 show the critical strain for initiation of dynamic recrystallization and strain to the peak stress respectively against Zener-Hollomon parameter, predicted [13, 14] using $Z = A\left[\sinh(\alpha\sigma)\right]^n = \dot{\varepsilon}\exp\frac{Q}{RT}$. Dynamic recrystallization in metals will involve some migration and rotation of grains. The ratio between critical strain and peak strain for dynamic recrystallization in both steels is approximately 0.9.

4 Conclusions

1. The peak observed in the stress-strain curve of alloy D9 stainless steels, for the tests conducted at 973–1073 K is attributed to dynamic recrystallization occurring in these materials.
2. Dynamic recovery is the dominant process, followed by dynamic recrystallization which is marked by a change in slope in the plot, flow stress against work hardening rate.

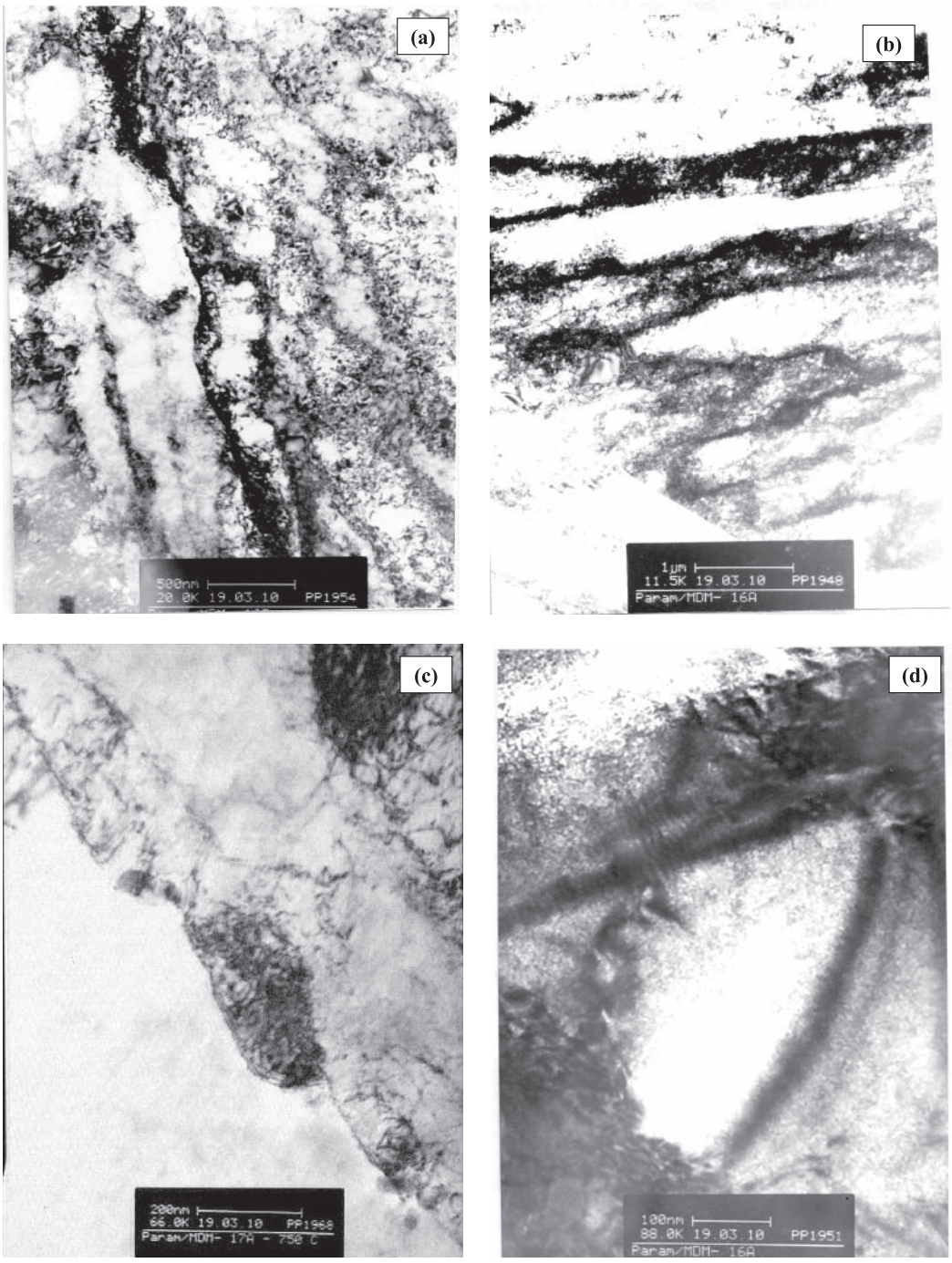

Fig. 8: TEM micrographs of ESR grade alloy D9 stainless steel (a) tested at 1073 K, depicting defect dominated elongated cells (b) tested at 1073 K, showing wavy nature of grain boundaries (c) tested at 1023 K, showing formation of subgrain boundaries along wavy grain boundary, and (d) tested at 1073 K, depicting fine recrystallized grains with moire fringes along its edge.

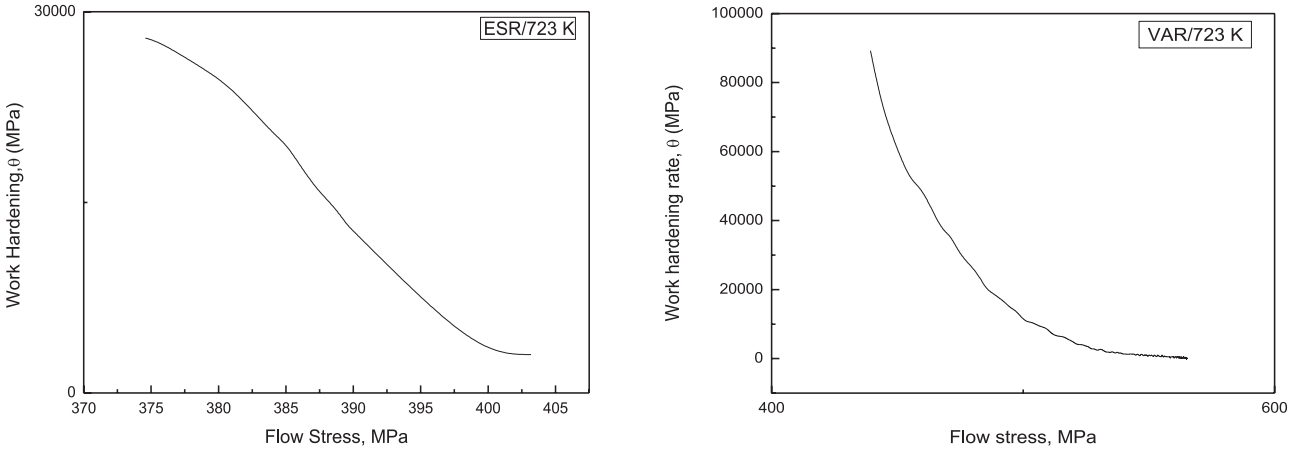

Fig. 9: Typical plots of work hardening rate as a function of flow stress in the non DRX regime.

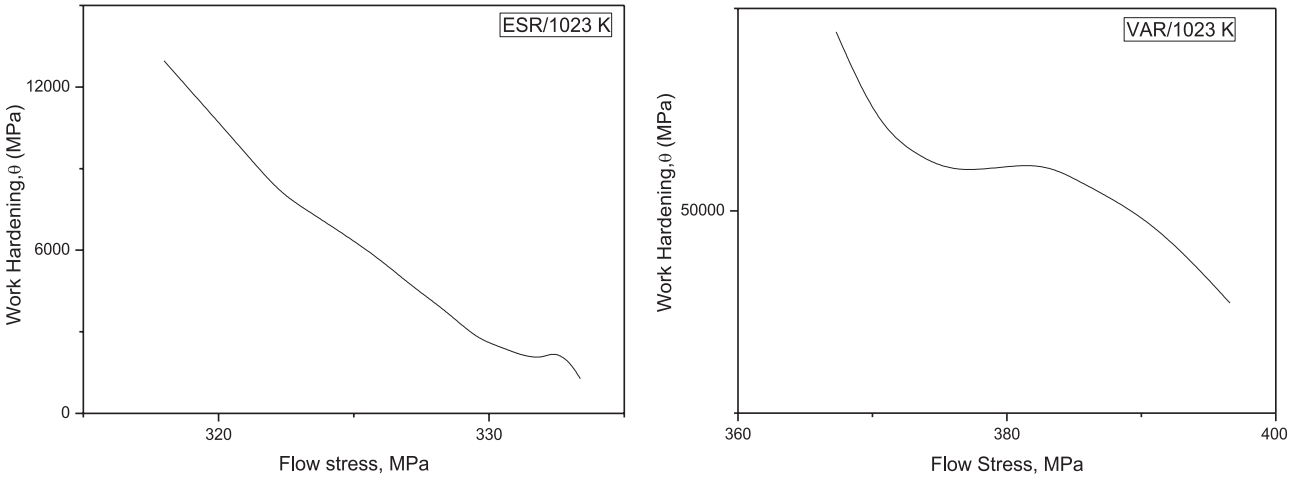

Fig. 10: Typical plots of work hardening rate as a function of flow stress in the DRX regime.

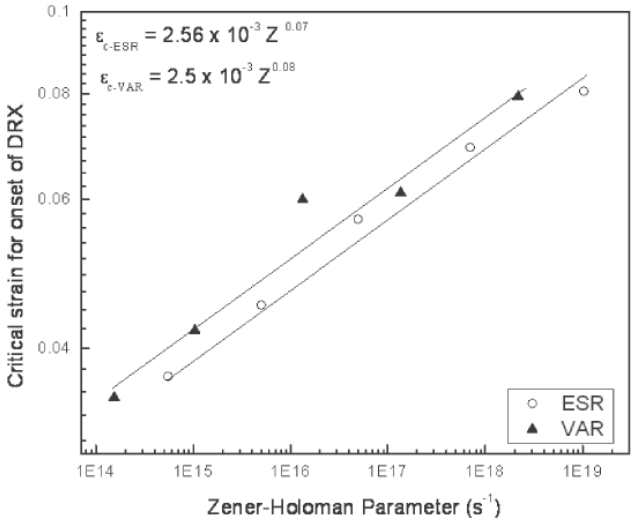

Fig. 11: Critical strain as a function of Zener–Hollomon parameter.

3. The values of the apparent activation energy evaluated as 384 kJ/mol for ESR grade and 372 kJ/mol for VAR grade, both called as alloy D9 stainless steel, agree well with that required for the dynamic recrystallization in both the steels.
4. The higher critical strain for onset of dynamic recrystallization in case of VAR alloy D9 stainless steel is due to smaller grain size.
5. The ratio between critical strain and peak strain for dynamic recrystallization is approximately 0.9 for both the steels.

Acknowledgments: The authors thank Dr. T. Jayakumar, Director, Metallurgy and Materials Programme for his support and guidance during the course of this study.

Received: October 18, 2012. Accepted: February 24, 2013.

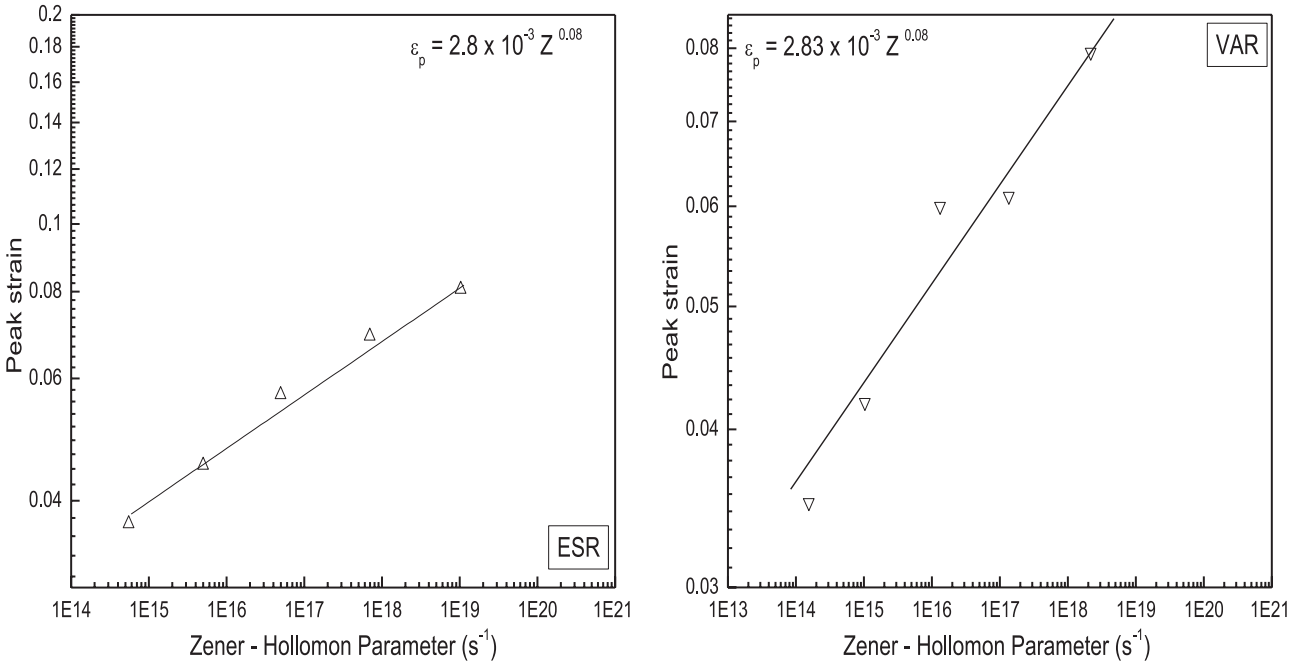

Fig. 12: Peak strain as a function of Zener–Hollomon parameter.

References

[1] Rodriguez P., Krishnan R. and Sundaram C.V., Bull. Mater. Sci. Vol. 6, No. 2, 339–367, 1984.

[2] Terlain A., Alamo A., Alwan F. and Foucher C., Proc. Internl. Conf. Materials for Nuclear Core Applications, BNES, 27–29 Oct. 1987, Bristol, UK, London, Vol. 1, p. 199, 1987.

[3] Maziaz P.J. and Roche T.K., J. Nucl. Mater., Vols. 103 & 104, 797–802, 1981.

[4] Montheillet F. and Jonas J.J., Recrystallization, Dynamic, Encyl. of App. Physics, Vol. 16, VCH Publishers Inc., 3-527-28138-X, 1996, pp. 205–225.

[5] Hertzberg R.W., Deformation and Fracture Mechanics of Materials, John Wiley and Sons, Inc, New York (1996), pp. 166–167.

[6] Nandagopal M., Parameswaran P., Vijayanand V.D., Laha K. and Mathew M.D., High Temperature Materials and Processes, Vol. 30, No. 3, pp. 229–232 (online).

[7] Samuel K.G., Ray S.K. and Sasikala G., Journal of Nuclear Materials, 355(1–3), pp. 30–37.

[8] Sivaprasad P.V., Venugopal S. and Venkadesan S., Metall. and Mater. Trans., 1997, pp. 171–178.

[9] Hebsur M.G., Abraham K.P. and Prasad Y.V.R.K., Journal of Mechanical Working Technology 341, 4 (1981).

[10] Dehghan-Manshadi A., Barnett M.R. and Hodgson P.D., Materials Science & Engineering A 485, p. 664 (2008).

[11] Kim S.I., Ko B.C., Lee C.M., Hwang S.K. and Yoo Y.C., Materials Science and Technology, 19, p. 1648 (2003).

[12] Wang Y., Shao W.Z., Zhen L., Yang C. and Zhang X.M., Journal of Alloys and Compounds 471, p. 331 (2009).

[13] Elwazri A.M., Wanjara P. and Yue S., Mater. Sci. Engg. A, 339, pp. 209–215 (2003).

[14] Ryan N.D. and McQueen H.J., Canad. Metall. Qutly., Vol. 29, No. 2, pp. 147–162 (1990).